Chapter 3

FTLE, LCS, and Five Examples

Here we review the method of extracting Lagrangian Coherent Structures (LCS) using the method of Finite Time Liapunov Exponents (FTLE). The method was first developed by Haller [Haller 2000], and further references that provide more detail include [Shadden 2005] and [Lekien 2007]. The underpinning premise in the FTLE method is that coherent structures in a turbulent flow are best characterized and identified by the surfaces of greatest separation. This Lagrangian approach, which uses particle trajectories that necessarily encode the time-dependence in the velocity field, is more effective in identifying persistent coherent structures than methods that utilize only Eulerian criteria. The method has the advantages that it is directly applicable to aperiodic flows, and to flows that are defined by discrete data sets over a finite time interval.

After reviewing the basic definitions, we will briefly examine five examples that illustrate various features of the method for a variety of flows.

3.1 FTLE and LCS

The discussion here will be with regard to two-dimensional flows in the plane, although this can be generalized to flows in n-dimensions, and to flows on manifolds [Lekien 2007]. We take the approach that the Eulerian velocity field describing the flow is given at the outset, either as an explicit analytical model, or as the result of integrating primitive equations for the flow (Navier-Stokes, for example), or from

interpolations of direct observations and measurements of the flow. The flow may correspond to an actual fluid flow, or the flow in the phase space of a dynamical system.

Since the FTLE method is a Lagrangian approach, we will need to compute the flow map that maps particles forward along their trajectories. Differentiation of the flow map will provide a measure of separation under the action of the flow. Finally, we define the LCS to be the surfaces in the flow on which separation is locally maximal.

Let the open set $D \subset \mathbb{R}^2$ be the domain of interest in the flow, and let $\mathbf{v}(\mathbf{x}, t)$ be a smooth time-dependent vector field on D that we refer to as the *velocity field*. At each time t, the velocity field assigns to each point $\mathbf{x} \in D$, a tangent vector from $T_{\mathbf{x}}D$. A *trajectory*, $\mathbf{q}(t; \mathbf{x}_0, t_0)$, is the unique curve in D parametrized by time that passes through the initial condition $\mathbf{x}_0 \in D$ at time t_0, and whose tangent vectors satisfy the vector field $\mathbf{v}$:

$$\frac{d\mathbf{q}(t; \mathbf{x}_0, t_0)}{dt} = \mathbf{v}(\mathbf{q}(t; \mathbf{x}_0, t_0), t)$$

for all times t. In the applications, the trajectory is obtained by numerically integrating the velocity field, using a Runge-Kutta scheme, for example.

Let $\phi_{t_0}^{t_0+t} : D \to D$ be the *flow map* associated with the vector field, so that

$$\phi_{t_0}^{t_0+t}(\mathbf{x}_0) := \mathbf{q}(t_0 + t; \mathbf{x}_0, t_0)\,.$$

For a smooth velocity field, $\phi_{t_0}^{t_0+t} : D \to D$ is a smooth map that depends on both the time, t_0, and the time of integration, t. Clearly, $\phi_{t_0}^{t_0} : D \to D$ is the identity map on D.

The flow map encodes the Lagrangian paths of particles, and provides access to the amount of local stretching in the flow. To this end, we use the linearization of the flow map,

$$\mathbf{x} \to D\phi_t^{t+T}(\mathbf{x})\,, \tag{3.1}$$

represented by a 2×2 matrix, to define the Cauchy-Green deformation tensor:

$$\Delta := \left[D\phi_t^{t+T}(\mathbf{x})\right]' D\phi_t^{t+T}(\mathbf{x}) \,, \tag{3.2}$$

where A' indicates the transpose of the matrix A. The adorning symbols on Δ have been dropped to avoid notational clutter, but it is understood that Δ assigns to each point in the domain D a time-dependent 2×2 matrix. Furthermore, Δ is everywhere positive definite and hence has positive eigenvalues. The deformation tensor contains information about the amount of (linearized) stretching in the flow. If the largest eigenvalue of Δ is greater than unity, then the eigenvector associated with this eigenvalue provides the direction in which the largest separation will occur. Thus, the eigenvalues of Δ provide a measure of the rate of separation. Accordingly, the Finite Time Liapunov Exponent, $\sigma_T(\mathbf{x}, t)$, is a time-dependent scalar field defined using the maximum eigenvalue of Δ:

$$\sigma_T(\mathbf{x}, t) := \frac{1}{2|T|} \ln \lambda_{\max}(\Delta) \,. \tag{3.3}$$

When convenient, we sometimes drop the notation indicating the dependencies, and write just σ. The FTLE defined in this way is a measure of the separation of trajectories induced by the flow over the interval of time $(t, t+T)$ with values of the FTLE greater than zero representing separation.

Following [Shadden 2005], we define the LCS to be locally maximizing surfaces, or "ridges", in the scalar field σ_T. In practice, the intuitive definition of "ridge" suffices to identify the LCS; however, in order to provide a precise mathematical definition, we must first introduce the notion of curvature of the surface σ, by defining the 2×2 Hessian matrix Σ:

$$\Sigma := D^2 \sigma_T(\mathbf{x}, t) \,. \tag{3.4}$$

By equality of mixed partial derivatives, Σ is a real symmetric matrix, and consequently has real eigenvalues and orthogonal eigenvectors. We label the smallest eigenvalue of Σ, $\lambda_{\mathbf{n}}$, and the associated eigenvector, $\mathbf{n}$. Then, we define the LCS to

be the set of all points in the domain for which the following two conditions hold:

C1. $\lambda_{\mathbf{n}} < 0\,,$

C2. $\nabla\sigma \cdot \mathbf{n} = 0\,.$

Taken together, these conditions define a curve in D that moves in time. As we shall see in the forthcoming examples, the LCS defined in this way for a wide range of flows are remarkably sharp, indicating that separation is generally not a diffuse property and is concentrated along LCS curves.

The definition of FTLE admits both positive and negative flow times T. For positive values of T, the FTLE measures separation forward in time and yields LCS that act as *repelling* surfaces; while for negative values of T, the FTLE measures separation backward in time, and hence yields LCS that act as *attracting* surfaces in forward time.

The LCS as defined above are co-dimension one surfaces of greatest separation. From a broader perspective, it is understood that these LCS curves are then used to identify the relevant coherent structures in a flow. For instance, the LCS may define the boundaries of an ocean eddy, whereas from the user's point of view, the eddy itself is the coherent structure of interest.

From a practical standpoint, the FTLE is computed numerically by placing a Cartesian grid of particles covering the flow region D. The flow map is then approximated by integrating all the particle trajectories forward in time. Differentiation of the flow map is performed via finite differencing to yield the FTLE at each point in D. The procedure is then repeated at subsequent time intervals in order to discover the time evolution of σ.

Increasing the integration time T tends to sharpen the ridges and extend their length in space. Typically, choosing a value for T is motivated by the relevant time-scales in the flow; T must be chosen long enough so that the important dynamics in the flow have sufficient time to induce separation. Choosing a value of T too large leads to too many LCS to be sensible. The choice of the integration time T is thus also tied to the relevant length scales that are most active in the flow. In practice, if the

given velocity field covers the temporal and spatial scales of interest, then choosing a suitable value of T is seldom an issue.

To complete this overview of LCS, we now provide five examples of FTLE fields and their corresponding LCS for a wide range of flow regimes.

3.2 The simple pendulum

To begin, we investigate the FTLE for the flow in the phase space of the simple pendulum. This is an elementary example (the flow is not even time-dependent!), but will be illustrative of the main features of LCS, and will also raise important non-trivial issues that will be addressed in later chapters.

The state of the simple pendulum is described by the angle of the pendulum with the vertical, θ, and its angular velocity, ω. The evolution of the flow through (θ, ω)-phase space is given by:

$$\begin{aligned} \dot{\theta}(t) &= \omega(t) \\ \dot{\omega(t)} &= -\sin\theta(t)\,, \end{aligned}$$

and the velocity field is shown in Figure 3.1(a).

The corresponding repelling FTLE field for an integration time of 11 time units is shown in Figure 3.1(b). The LCS are easily discernible ridges in the FTLE, and separate regions in which the pendulum motion is a back-and-forth oscillation, from regions of running windmill behavior. Computing the FTLE for integration backward in time yields the attracting FTLE field in Figure 3.1(c). Taken together, the repelling LCS and the attracting LCS enclose the region of oscillating motion. Thus, the LCS act as *separatrices* in that they separate regions of the flow with qualitatively different behavior. Also, we observe that increasing the integration time "grows" the manifold, since more trajectories that begin closer to the unstable vertical equilibrium point will have the opportunity to separate.

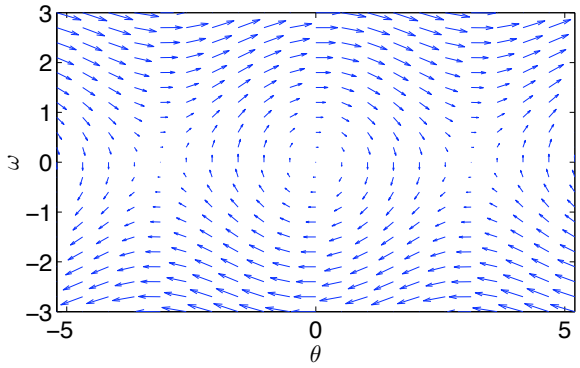

(a) Velocity field for the simple pendulum.

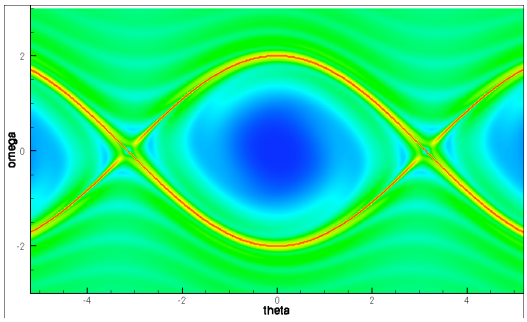

(b) Repelling FTLE for the simple pendulum flow. The LCS are sharp ridges that separate regions of oscillatory motion from regions of "running" motion.

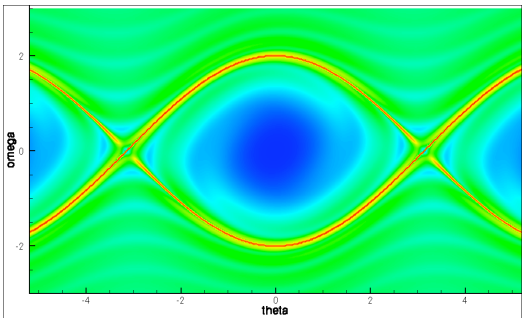

(c) When combined with the LCS in the attracting FTLE field shown here, the LCS fully enclose the region of oscillatory motion.

Figure 3.1: FTLE and LCS in the flow of the simple pendulum.

3.3 Monterey Bay

In this example, we analyze the flow defined by output from a nested ocean model for two-dimensional surface flow in a coastal region near Monterey Bay, California provided by Chao (see [Li 2008] for details of the model). In the figures below, the FTLE scalar fields in both forward and backward time directions have been computed, and then plotted as an overlaid filled contour plot using windowing of the fields to reveal only the regions of strongest repulsion and attraction. Colored drifters are also placed in the flow to indicate their motion relative to LCS.

The sequence of images reveals properties of the LCS that recur for a wide-range of flows. These are:

- The LCS delineate regions that have different dynamical fates – brown drifters re-circulate near the coast, while green drifters are flushed out to sea.
- Intersections of the attracting and repelling LCS define strongly hyperbolic points in the flow.
- The LCS are almost inariant, in that very little fluid crosses the LCS.
- The LCS act as barriers to transport, and reveal pathways by which transport occurs.

The LCS computed for coastal regions can be used to guide the placement of drifters for measuring ocean data so that the drifters recirculate within the region of interest and achieve better coverage. An experiment to implement this approach is being conducted in July and August, 2009, in Prince William Sound, Alaska, where the modeling of the transport of oil spills due to ocean currents in the sound is of particular interest. The LCS can also be used to recognize persistent structures in coastal waters such as eddies separating off coastal protrusions. In a separate study, [Lekien 2005] has investigated the use of LCS to mitigate the effect of pollution discharges by ensuring that effluent is released at times when there are no transport barriers to prevent pollutants from being quickly flushed out to sea.

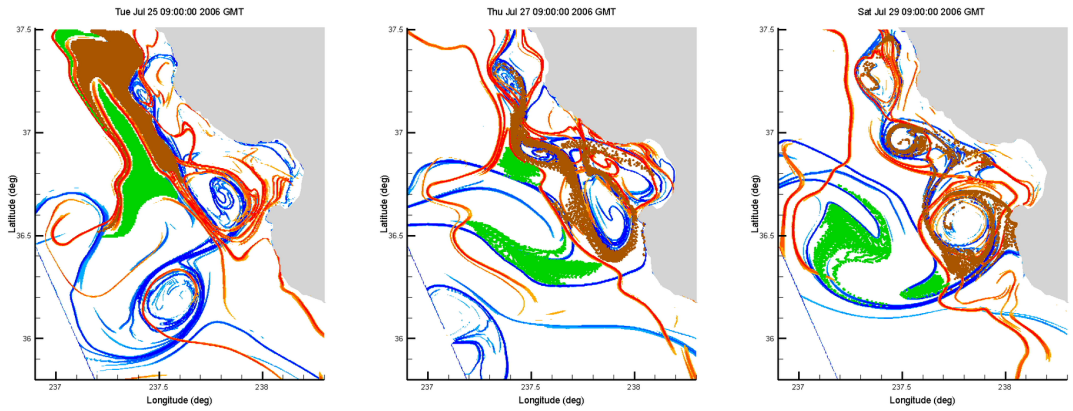

Figure 3.2: LCS near Monterey Bay are depicted here at 48 hour intervals. The attracting LCS (blue curves) and the repelling LCS (red curves) define the boundaries of vortices as well as lobes colored green and brown. Since no fluid crosses the LCS, transport and mixing occurs via the motion of the lobes. The green lobes are flushed out to sea while the brown lobes recirculate near the coast.

3.4 The atmosphere of Titan

Images recently returned from the Cassini and Huygens missions to Saturn's moon, Titan, have spurred great interest in further exploring the meteorology of Titan's dense atmosphere, hydrological cycle, and hydrocarbon lakes. Designs for Montgolfiere balloons are currently under consideration as the observing platform of choice for exploring the Titan environment. With limited onboard propulsion, the venturing capabilities of a balloon will depend largely on the transport structures present in the Titan atmosphere. Consequently, design engineers will need to consider whether, for example, there are barriers to transport into and out of the polar regions, or if there are regions of potential entrapment, or if wind reversals as a function of altitude will allow for navigation with the aid of a small amount of vertical control authority.

We have computed three-dimensional LCS using the velocity fields in a Titan wind model provided by the authors of [Richardson 2007]. Figure 3.3(a) shows a sample constant-height section through the FTLE field. We observe turbulent structures in the mixing region between the retrograde equatorial flow, and the zonal flow in the upper latitudes. Furthermore, a strong repelling LCS encircles the northern polar region, indicating that travel to the pole during this time period will be impossible

using ambient winds alone. Blue and red drifters placed on either side of this separatrix enter different dynamical regimes: the blue drifters continue to rapidly circle the pole, while the red drifters enter a quiescent pocket closer to the equator. In a similar manner to the pendulum example, the LCS delineates a separation between regions with different dynamical outcomes.

3.5 Overflows in the North Atlantic

The thermohaline circulation is oceanic flow driven by buoyancy effects due to differences in temperature and salinity, and leads to global circulation of the oceans. The circulation transports and distributes large amounts of energy, and hence has paramount influence on the global climate. Indeed, conjectures have been made that global warming could cause the thermohaline circulation to cease, drastically affecting global climates - most especially the climate of Northern Europe [Vellinga 2002]. Thus, accurate global climate forecasting requires a through understanding of the transport mechanisms at play in the thermohaline circulation.

An important element of thermohaline transport is mixing that occurs in oceanic *overflows*, a process in which cold dense saline water descends below warmer less dense fresh water causing instability and mixing at the interface. Current global climate models have grid scales too large to resolve these mixing processes, and must resort to a parametrized model to capture their effects.

Odier has conducted laboratory experiments described in [Odier 2007] to replicate oceanic overflows and characterize the resulting turbulent mixing processes so that these effects may be included in global models. (For practical purposes, the experimental setup actually investigates the ascension of less dense fluid against an inclined plate, rather than the sinking of a cold dense fluid.) The fluid is initially passed over a propeller to induce turbulent flow and the flow field is imaged using particle image velocimetry.

In order to characterize mixing, the interface between the two fluids must first be determined, and then the amount of flux across this boundary must be measured.

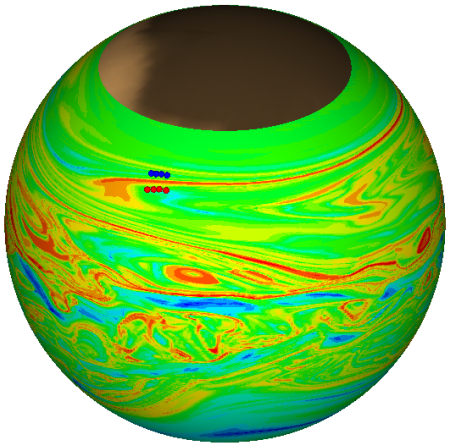

(a) The FTLE for the atmosphere of Titan. A repelling LCS acts as a barrier to transport to the North Pole.

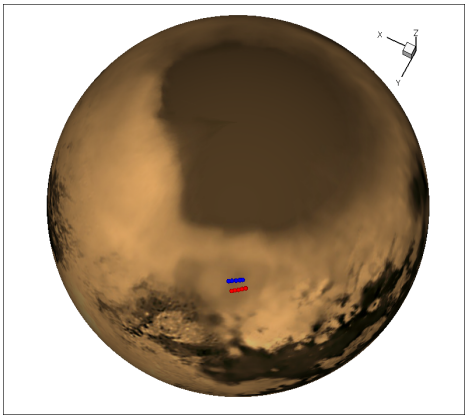

(b) Four particles are placed on either side of the repelling LCS.

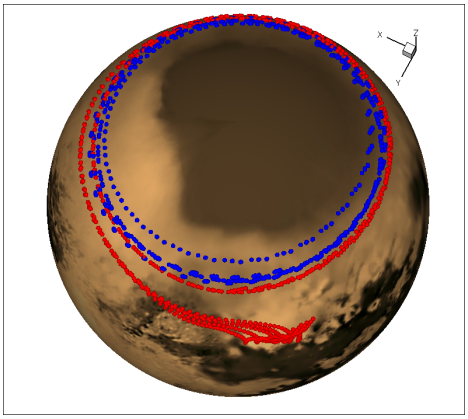

(c) The blue and red drifters separate. The blue drifters continue to circle the pole, while the red drifters enter a different flow regime closer to the equator.

Figure 3.3: LCS in the atmosphere of Titan.

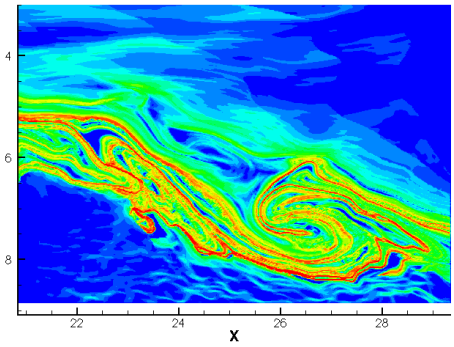

(a) Repelling FTLE. The LCS indicates the interface between the layers. Furthermore, the LCS indicates the lobe that will be *detrained* from the overflow above to the quiescent flow beneath.

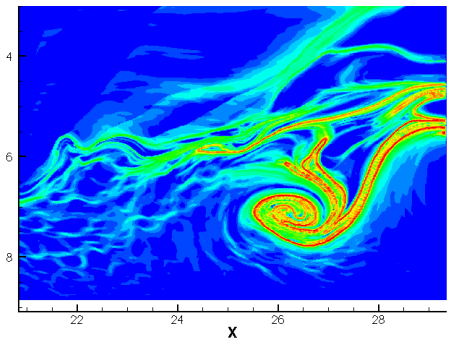

(b) Attracting FTLE. The LCS indicates a lobe that will be *entrained* into the overflow above.

Figure 3.4: LCS in experimental realizations of ocean overflows.

Not surprisingly, the identification of this boundary for the turbulent flow is not easily performed by viewing plots of traditional Eulerian fields. Velocity and vorticity plots are unhelpful and misleading.

We have computed LCS for flow data obtained during the overflow experiment with promising results. The repelling LCS shown in Figure 3.4(a) captures the turbulent mixing layer and shows the boundary between the less dense overflow moving to the right above the quiescent more dense fluid below. In Figure 3.4(a), we see that the LCS reveals not only the interface, but also the mechanisms by which mixing occurs: the LCS outlines a narrow tendril-shaped lobe that will be detrained into the quiescent flow beneath, while fluid exterior to the lobe will exit the flow at top right. Similarly, the attracting LCS plotted in Figure 3.4(b) demarcates a lobe in the quiescent flow that will be entrained into the overflow above. In this way, LCS can be used to quantify detrainment and entrainment. In fact, to the extent that the flow is planar, the areas of the lobes correlate with the amount of mixing occuring across the interface.

3.6 The elliptic three-body problem

Koon has shown that careful consideration and utilization of invariant manifolds in the circular restricted three-body problem can reveal energy efficient pathways for transport in the solar system [Koon 2000]. Specifically, the stable and unstable manifolds of the periodic orbits, associated with Lagrange points in the restricted three-body problem, form tubes through which trajectories traveling from one region of phase space to another must pass. Desired itineraries are obtained by finding intersections between tubes traveling to and from the relevant regions.

Computing these invariant manifolds typically requires intensive computation of high order normal forms (above 20^{th} order for example), inserting initial conditions infinitesimally displaced in the stable and unstable directions, and then integrating forward and backward in time in accordance with the classical dynamical systems definition of stable and unstable manifolds. Adopting a different approach, we utilize the property that the invariant manifolds are also separatrices in the flow. Hence, we can compute the LCS to directly discover the tubes through which trajectories must pass. The versatility of the LCS method allows for computations of these manifolds even in the case of the elliptic restricted three-body problem in which the eccentricity of the primary orbits yields non-autonomous equations of motion [Gawlik 2009]. Moreover, the LCS method allows for the computation of these manifolds for the solar system using the aperiodic flow induced by the entire ephemeris.

Since the Jacobi integral is absent in the elliptic problem, we cannot project onto an energy surface and must integrate trajectories in the full four-dimensional phase space. To compute the LCS, we initialize trajectories on a three-dimensional Poincaré section ($y = 0$), integrate them forward in the four-dimensional space, and compute the FTLE. Figure 3.5(a) shows a still image of the time-dependent FTLE on this three-dimensional section, while Figure 3.5(b) is yet another section through this three-dimensional space onto the $(x, \dot{x})$-plane. The resulting LCS demarcate pockets of initial conditions that undergo different dynamical behavior – for instance, those outside the pocket remain in an orbit interior to Jupiter, while those inside the pocket

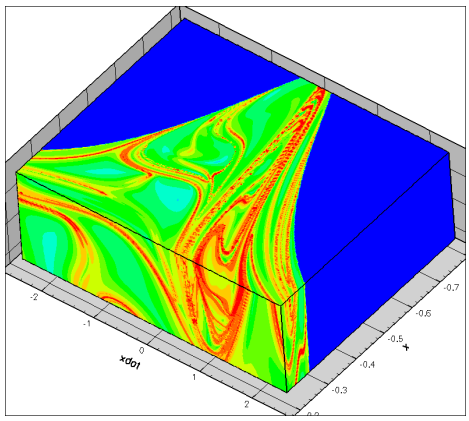

(a) A 3D section of the 4D FTLE for the elliptic three-body problem.

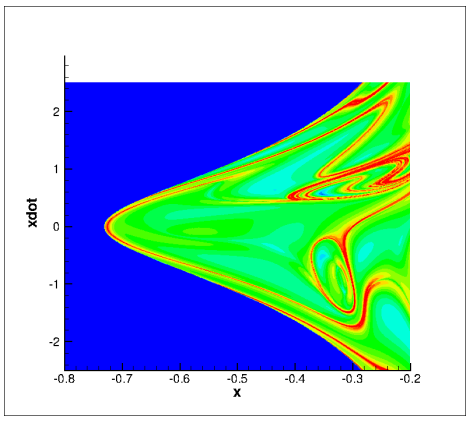

(b) A 2D section of the 4D FTLE for the elliptic three-body problem. Notice that the LCS cut out regions, or "tubes," in phase space.

Figure 3.5: LCS for the elliptic three-body problem.

escape Jupiter's orbit to an exterior orbit.